


# Suppression of the vapor cell temperature error in a spin-exchange relaxation-free comagnetometer

Jia-Li Liu(刘佳丽), Li-Wei Jiang(姜丽伟), Chi Fang(方驰), Xin Zhao(赵鑫), and Yuan-Qiang Chen(陈远强)

**Citation:**Chin. Phys. B, 2024, 33 (**12**): 120701. DOI: 10.1088/1674-1056/ad84ce
Journal homepage: http://cpb.iphy.ac.cn; http://iopscience.iop.org/cpb

**What follows is a list of articles you may be interested in**

---

## Performance optimization of a SERF atomic magnetometer based on flat-top light beam

Ziqi Yuan(袁子琪), Junjian Tang(唐钧剑), Shudong Lin(林树东), and Yueyang Zhai(翟跃阳)
Chin. Phys. B, 2024, 33 (**6**): 060703. DOI: 10.1088/1674-1056/ad401b

## A compact and closed-loop spin-exchange relaxation-free atomic magnetometer for wearable magnetoencephalography

Qing-Qian Guo(郭清乾), Tao Hu(胡涛), Xiao-Yu Feng(冯晓宇), Ming-Kang Zhang(张明康), Chun-Qiao Chen(陈春巧), Xin Zhang(张欣), Ze-Kun Yao(姚泽坤), Jia-Yu Xu(徐佳玉),Qing Wang(王青), Fang-Yue Fu(付方跃), Yin Zhang(张寅), Yan Chang(常严), and Xiao-Dong Yang(杨晓冬)
Chin. Phys. B, 2023, 32 (**4**): 040702. DOI: 10.1088/1674-1056/ac7e38

## Suppression of laser power error in a miniaturized atomic co-magnetometer based on split ratio optimization

Wei-Jia Zhang(张伟佳), Wen-Feng Fan(范文峰), Shi-Miao Fan(范时秒), and Wei Quan(全伟)
Chin. Phys. B, 2023, 32 (**3**): 030701. DOI: 10.1088/1674-1056/ac81b1

## A synthetic optically pumped gradiometer for magnetocardiography measurements

Shu-Lin Zhang(张树林), Ning Cao(曹宁)
Chin. Phys. B, 2020, 29 (**4**): 040702. DOI: 10.1088/1674-1056/ab7801

## Miniature quad-channel spin-exchange relaxation-free magnetometer for magnetoencephalography

Jian-Jun Li(李建军), Peng-Cheng Du(杜鹏程), Ji-Qing Fu(伏吉庆), Xu-Tong Wang(王旭桐), Qing Zhou(周庆), Ru-Quan Wang(王如泉)
Chin. Phys. B, 2019, 28 (**4**): 040703. DOI: 10.1088/1674-1056/28/4/040703

---

# Suppression of the vapor cell temperature error in a spin-exchange relaxation-free comagnetometer

Jia-Li Liu(刘佳丽)[1], Li-Wei Jiang(姜丽伟)[2,3,†], Chi Fang(方驰)[2,3], Xin Zhao(赵鑫)[1], and Yuan-Qiang Chen(陈远强)[1]

[1] *National Institute of Extremely-Weak Magnetic Field Infrastructure, Hangzhou* 310051, *China*
[2] *Institute of Large-scale Scientific Facility and Centre for Zero Magnetic Field Science, Beihang University, Beijing* 100191, *China*
[3] *Zhejiang Provincial Key Laboratory of Ultra-Weak Magnetic-Field Space and Applied Technology, Hangzhou Innovation Institute, Beihang University, Hangzhou* 310051, *China*

(Received 1 August 2024; revised manuscript received 12 September 2024; accepted manuscript online 9 October 2024)

The fluctuation of the vapor cell temperature leads to the variations of the density of the alkali metal atoms, which seriously damages the long-term stability of the spin-exchange relaxation-free (SERF) comagnetometer. To address this problem, we propose a novel method for suppressing the cell temperature error by manipulating the probe laser frequency. A temperature coefficient model of the SERF comagnetometer is established based on the steady-state response, which indicates that the comagnetometer can be tuned to a working point where the output signal is insensitive to the cell temperature fluctuation, and the working point is determined by the relaxation rate of the alkali metal atoms. The method is verified in a K–Rb–$^{21}$Ne comagnetometer, and the experimental results are consistent with the theory. The theory and method presented here lay a foundation for the practical applications of the SERF comagnetometer.

**Keywords:** spin-exchange relaxation-free, atomic comagnetometer, cell temperature error, probe laser frequency

**PACS:** 07.07.Df, 07.55.Ge, 42.79.–e **DOI:** 10.1088/1674-1056/ad84ce

## 1. Introduction

The alkali metal–noble gas comagnetometer has found a wide spectrum of applications in the fundamental physics, geodesy, and inertial navigation with the development of the quantum precision measurement technology.[1–4] One of the most promising comagnetometer is the spin-exchange relaxation-free (SERF) comagnetometer due to the ultrahigh theoretical precision and possibilities of miniaturization.[5–7] The SERF comagnetometer is presented by Romalis group based on a K–$^3$He spin ensemble for the first time in 2005.[8] Since then, an intense research effort is devoted to improve the sensitivity and long-term stability of the SERF comagnetometer.[9–12] At present, a rotation sensitivity of $2.1\times10^{-8}$ (rad/s)/Hz$^{1/2}$ and a bias drift of $10^{-2}$ °/h are realized in a K–Rb–$^{21}$Ne comagnetometer.[13,14]

The SERF comagnetometer, consists of the spin coupled ensemble of the alkali metal and noble gas atoms, senses the inertial rotation with a high precision by detecting the precession of the noble gas atoms utilizing the alkali metal atoms operated in SERF regime.[15] The high density of the alkali metal atoms is one of the essential conditions to operate the alkali metal atoms in SERF regime and contributes to enhance the response of the comagnetometer, which can be realized by maintaining the alkali metal atoms at high temperature.[16] Nonetheless, the fluctuation of the vapor cell temperature leads to the variation of the density of the alkali metal atoms,[17,18] which further causes the variation of the polarizations of the electron spins and nuclear spins,[19] and eventually results in the drift of the output of the SERF comagnetometer. Therefore, the vapor cell temperature error is an important limiting factor to improve the long-term stability of the SERF comagnetometer.[20] In general, the vapor cell temperature error can be suppressed by improving the precision of temperature control system or reducing the sensitivity of the comagnetometer to the temperature fluctuation.[21,22] With the improvement of the performance of the comagnetometer, the precision of the temperature control system needs to be increasingly high. The promotion of the precision of temperature control system is finite, which limits the further improvement of the precision of the comagnetometer. The method for reducing the sensitivity to the temperature fluctuation is more hopeful to suppress the cell temperature error. For convenience, the coefficient of the output signal of the comagnetometer changing with the cell temperature is defined as the temperature coefficient, which can reflect the sensitivity of the output signal to the temperature fluctuation. It has been presented that the temperature coefficient for the SERF comagnetometer can be reduced by adjusting the cell temperature or pump laser power.[20,23] However, by using this method, the temperature or pump laser power needs to be tuned in a large range to find the zero point of the temperature coefficient, which is time-consuming because it takes several hours for the coupled en-

†Corresponding author. E-mail: jiangliwei@buaa.edu.cn

© 2024 Chinese Physical Society and IOP Publishing Ltd 

semble to reach a stable state when the temperature or pump laser power is changed a lot. In addition, the method to reduce temperature coefficient for the SERF magnetometer has been presented by setting the optical depth (OD) of the probe laser close to one,[24] which is a promising method for suppressing the temperature error, while the method has not been applied in the SERF comagnetometer and the related theory and manipulation method are urgently need to be established.

In this paper, we propose a novel method for suppressing the vapor cell temperature error of the SERF comagnetometer by manipulating the probe laser frequency. In order to analyze the impact of temperature fluctuation on the output signal, a temperature coefficient model of the SERF comagnetometer is established based on the steady-state response. According to the model, we found that the comagnetometer can be tuned to a working point where the output signal is insensitive to the cell temperature fluctuation, and the working point is determined by the relaxation rate of the alkali metal atoms. Then, the method is verified in a K–Rb–$^{21}$Ne comagnetometer. The theory and method presented here are of great significance to improve the performance of the SERF comagnetometer.

## 2. Principle and method

The dynamics of the spin ensembles of the electron spins and nuclear spins is the foundation of the SERF comagnetometer for rotation sensing, which can be phenomenologically described by a set of Bloch equations.[25] The evolution of the electron spin polarization $\boldsymbol{P}^{\mathrm{e}}$ and the nuclear spin polarization $\boldsymbol{P}^{\mathrm{n}}$ can be described as follows:[8,26]

$$\begin{aligned}\frac{\partial \boldsymbol{P}^{\mathrm{e}}}{\partial t} &= \frac{\gamma_{\mathrm{e}}}{Q}\left(\boldsymbol{B}+\lambda M^{\mathrm{n}}\boldsymbol{P}^{\mathrm{n}}+\boldsymbol{L}\right)\times\boldsymbol{P}^{\mathrm{e}}+\boldsymbol{\Omega}\times\boldsymbol{P}^{\mathrm{e}}\\ &\quad+\frac{\left(R_{\mathrm{p}}\boldsymbol{s}^{\mathrm{p}}+R_{\mathrm{se}}^{\mathrm{en}}\boldsymbol{P}^{\mathrm{n}}+R_{\mathrm{m}}\boldsymbol{s}^{\mathrm{m}}-R_{\mathrm{tot}}^{\mathrm{e}}\boldsymbol{P}^{\mathrm{e}}\right)}{Q\left(\boldsymbol{P}^{\mathrm{e}}\right)},\\ \frac{\partial \boldsymbol{P}^{\mathrm{n}}}{\partial t} &= \gamma_{\mathrm{n}}\left(\boldsymbol{B}+\lambda M^{\mathrm{e}}\boldsymbol{P}^{\mathrm{e}}\right)\times\boldsymbol{P}^{\mathrm{n}}+\boldsymbol{\Omega}\times\boldsymbol{P}^{\mathrm{n}}\\ &\quad+R_{\mathrm{se}}^{\mathrm{ne}}\boldsymbol{P}^{\mathrm{e}}-R_{\mathrm{tot}}^{\mathrm{n}}\boldsymbol{P}^{\mathrm{n}}.\end{aligned}\tag{1}$$

The first term describes the precession of the electron spins and nuclear spins. The electron spins precess in the ambient magnetic field $\boldsymbol{B}$, the polarized magnetic field of the nuclear spins $\lambda M^{\mathrm{n}}\boldsymbol{P}^{\mathrm{n}}$ and the light shift $\boldsymbol{L}$. Similarly, the nuclear spins precess in the ambient magnetic field $\boldsymbol{B}$ and the polarized magnetic field of the electron spins $\lambda M^{\mathrm{e}}\boldsymbol{P}^{\mathrm{e}}$. $\gamma_{\mathrm{e}}$ and $\gamma_{\mathrm{n}}$ are the gyromagnetic ratios of the electron spins and nuclear spins, respectively. $Q$ is the slowing-down factor, which is a function of the electron spin polarization.[27] The second term is the rotation term, where $\boldsymbol{\Omega}$ is the input inertial rotation. The third term is the relaxation term. $R_{\mathrm{tot}}^{\mathrm{e}}$ and $R_{\mathrm{tot}}^{\mathrm{n}}$ are the total relaxation rates of the electron spins and nuclear spins. $R_{\mathrm{tot}}^{\mathrm{e}}$ consists of the pumping rates $R_{\mathrm{p}}$ and $R_{\mathrm{m}}$, the total spin-destruction relaxation rate $R_{\mathrm{sd}}^{\mathrm{e}}$ and the spin-exchange rate from nuclear spins to electron spins $R_{\mathrm{se}}^{\mathrm{en}}$. $R_{\mathrm{p}}$ and $R_{\mathrm{m}}$ are the pumping rates from the pump laser and probe laser, which are determined by the power density and frequency of the laser. $\boldsymbol{s}^{\mathrm{p}}$ and $\boldsymbol{s}^{\mathrm{m}}$ represent the degree of circular polarization. The total spin-destruction relaxation $R_{\mathrm{sd}}^{\mathrm{e}}$ can be described as $R_{\mathrm{sd}}^{\mathrm{e}}=R_{\mathrm{sd}}^{\mathrm{ee}}+R_{\mathrm{sd}}^{\mathrm{en}}+R_{\mathrm{sd}}^{\mathrm{eq}}=n_{\mathrm{e}}\sigma_{\mathrm{sd}}^{\mathrm{ee}}\bar{v}^{\mathrm{ee}}+n_{\mathrm{n}}\sigma_{\mathrm{sd}}^{\mathrm{en}}\bar{v}^{\mathrm{en}}+n_{\mathrm{q}}\sigma_{\mathrm{sd}}^{\mathrm{eq}}\bar{v}^{\mathrm{eq}}$, where $R_{\mathrm{sd}}^{\mathrm{ee}}$, $R_{\mathrm{sd}}^{\mathrm{en}}$, and $R_{\mathrm{sd}}^{\mathrm{eq}}$ are the relaxations caused by the collisions with alkali atoms, noble gas atoms, and the quenching gas atoms. $n_{\mathrm{e}}$, $n_{\mathrm{n}}$, and $n_{\mathrm{q}}$ are the densities of the alkali metal atoms, the noble gas, and quenching gas atoms. $\sigma_{\mathrm{sd}}^{\mathrm{ee}}$, $\sigma_{\mathrm{sd}}^{\mathrm{en}}$, and $\sigma_{\mathrm{sd}}^{\mathrm{eq}}$ are the spin-destruction cross sections for different colliding pairs. $\bar{v}$ is the mean relative velocity, which differs between colliding pairs. Similarly, $R_{\mathrm{se}}^{\mathrm{en}}=n_{\mathrm{n}}\sigma_{\mathrm{se}}^{\mathrm{en}}\bar{v}^{\mathrm{en}}$, where $\sigma_{\mathrm{se}}^{\mathrm{en}}$ is the spin-exchange cross section for alkali metal and noble gas atoms. According to the saturated vapor pressure formula $n_{\mathrm{e}}=\left(10^{21.866+A-B/T}\right)/T$, the density of the alkali metal atoms $n_{\mathrm{e}}$ is directly determined by the cell temperature $T$.[17] Whereas the densities of the noble gas and quenching gas atoms are determined by the initial pressure, which are hardly affected by the fluctuations of the cell temperature. Therefore, the fluctuation of the cell temperature mainly affects the spin-destruction relaxation rate $R_{\mathrm{sd}}^{\mathrm{ee}}$. Since the variation of mean relative velocity between atoms is 0.1%/K under our measurement condition, the temperature dependence of the mean relative velocity between atoms can be neglected. For convenience, the total electron spin relaxation can be defined as $R_{\mathrm{tot}}^{\mathrm{e}}=R_{\mathrm{sd}}^{\mathrm{ee}}+R_{\mathrm{rel}}^{\mathrm{iT}}$, where $R_{\mathrm{rel}}^{\mathrm{iT}}$ is the relaxation rate independent on the cell temperature.

The output signal of the SERF comagnetometer sensing the inertial rotation can be obtained by solving Eq. (1). Since the light shift can be zeroed by tuning the frequency of the laser to atomic resonance line or compensated by the longitudinal magnetic field,[28,29] the light shift is regarded as zero in the following analysis. The relaxation rate of the electron spins $R_{\mathrm{tot}}^{\mathrm{e}}$ is much larger than the relaxation rate of the nuclear spins $R_{\mathrm{tot}}^{\mathrm{n}}$, so the value of $R_{\mathrm{tot}}^{\mathrm{n}}$ can be ignored in the derivation.[30] In general, the spin ensembles in the SERF comagnetometer are polarized along $z$-axis by the pump laser, and the transverse components of the electron spin polarization are detected by the probe laser to obtain the inertial rotation. Supposing the probe laser is along $x$-axis, the electron spin polarization in the $x$ direction can be acquired as follows:

$$P_x^{\mathrm{e}}=\frac{\gamma_{\mathrm{e}}R_{\mathrm{p}}}{\gamma_{\mathrm{n}}\left(R_{\mathrm{sd}}^{\mathrm{ee}}+R_{\mathrm{rel}}^{\mathrm{iT}}\right)^2}\Omega_y.\tag{2}$$

According to Eq. (2), the electron spin polarization $P_x^{\mathrm{e}}$ is proportional to $\Omega_y$. In the comagnetometer, $P_x^{\mathrm{e}}$ can be measured by the optical rotation angle of the linearly polarized probe laser using Faraday effect,[31] which is given by

$$\theta=-\frac{\pi}{2}ln_{\mathrm{e}}cr_{\mathrm{e}}P_x^{\mathrm{e}}f_{\mathrm{D1}}\,\mathrm{Im}\left[L\left(\nu_{\mathrm{pr}}-\nu_{\mathrm{Rb}}\right)\right].\tag{3}$$

Here $l$ is the optical path length. $c$ is the speed of light, $r_e$ is the classical radius of electron, and $f_{D1}$ is the oscillator strength.

$$L(\nu_{pr}-\nu_{Rb})=[\Gamma/2+\mathrm{i}\,(\nu_{pr}-\nu_{Rb})]/[(\nu_{pr}-\nu_{Rb})^2+\Gamma^2/4]$$

is the Lorentz function of the probe laser frequency, where $\Gamma$ is the pressure broadening of optical absorption curve, $\nu_{pr}$ is the probe laser frequency and $\nu_{Rb}$ is the natural resonant frequency of Rb atoms. Taking into account absorption of the probe laser, the output signal of the comagnetometer can be described as

$$V_{out}=K_s I_i \theta\, \mathrm{e}^{-OD}, \tag{4}$$

where $K_s$ is the conversion coefficient, $I_i$ is the probe laser power before the cell. $OD$ is the optical depth of the probe laser, which is a function of the probe laser frequency $\nu_{pr}$ and can be shown as follows:

$$OD=n_e l c r_e f_{D1}\,\mathrm{Re}\left[L\left(\nu_{pr}-\nu_{Rb}\right)\right]. \tag{5}$$

According to the above analysis, the variation of the density of alkali metal atoms $n_e$ is the main term when the cell temperature fluctuates, which leads to the variations of the relaxation rate and polarization of the electron spins, and further results in the drift of output signal of the SERF comagnetometer. In order to study the influence of fluctuation of the cell temperature on the output signal, the derivation of the output signal to the cell temperature $T$ is defined as the temperature coefficient $K_T$, which is shown as follows:

$$\begin{aligned}K_T &= \frac{\partial V_{out}}{\partial n_e}\frac{\partial n_e}{\partial T}\\ &= -\frac{n_e\,(B\ln 10-T)\,\gamma_e P_x^e K_1 \Omega_y\,\mathrm{e}^{-OD}}{2\gamma_n T^2 {R_{tot}^e}^2}\\ &\quad\times\left[R_{sd}^{ee}\,(OD+1)+R_{rel}^{iT}\,(OD-1)\right],\end{aligned} \tag{6}$$

where $K_1=K_s I_i l r_e c f_{D1}\,\mathrm{Im}\left[L\left(\nu_{pr}-\nu_{Rb}\right)\right]$. The zero point of the temperature coefficient of SERF comagnetometer can be derived by setting the left-hand side of Eq. (6) to 0. When the $OD$ satisfies the condition in Eq. (7), the temperature coefficient is zero, which implies that the output signal of SERF comagnetometer is not changed with the variation of the cell temperature. Therefore, the sensitive of the output signal to the fluctuation of the cell temperature can be suppressed by manipulating the probe laser frequency.

$$OD=\frac{R_{rel}^{iT}-R_{sd}^{ee}}{R_{tot}^{e}}. \tag{7}$$

In order to further verify the results, the dependence of the temperature coefficient of SERF comagnetometer on the detuning frequency of probe laser from Rb D1 resonance line is simulated and shown in Fig. 1. The $OD$ as a function of the probe laser frequency is also plotted in Fig. 1. The simulations are based on the K–Rb–$^{21}$Ne comagnetometer with a typically temperature of 453 K. At this temperature, the relaxation rates $R_{sd}^{ee}$ and $R_{rel}^{iT}$ are calculated as 303.6 $\mathrm{s}^{-1}$ and 557.8 $\mathrm{s}^{-1}$. According to the simulation result, the temperature coefficient $K_T$ is zero when the detuning frequency is $\pm$170 GHz or within the range of $-$50 GHz to 50 GHz. In order to reduce the optical pumping introduced by the probe laser, the probe laser frequency is set to far detune from D1 resonance line of Rb atoms. The comagnetometer operates at the zero point of the temperature coefficient when the detuning frequency is $\pm$170 GHz, and the corresponding $OD$ is 0.29, which is consistent with the prediction of Eq. (7).

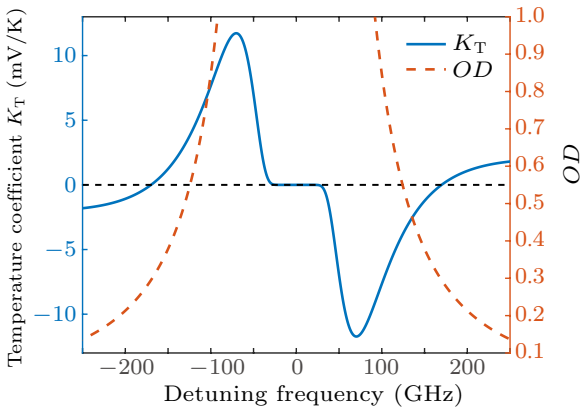



**Fig. 1.** Simulation of the temperature coefficients of the SERF comagnetometer as the function of the detuning frequency of probe laser from Rb D1 resonance line. When the $OD$ is equal to the ratio of the difference of the relaxation of the electron spins independent on temperature and the spin-destruction relaxation of electron spins to the total relaxation of the electron spins, the temperature coefficient reaches zero.

## 3. Experimental setup

The method for suppressing the cell temperature error is investigated in a K–Rb–$^{21}$Ne comagnetometer, whose schematic is shown in Fig. 2. The center of the comagnetometer is an 8-mm-diameter aluminosilicate glass cell, which contains a mixture of Rb atoms and K atoms, 2-atm (1 atm = $1.01325\times10^5$ Pa) $^{21}$Ne for providing the nuclear spins and 60-Torr (1 Torr = $1.33322\times10^2$ Pa) $N_2$ for quenching. The high alkali-metal atoms density and near-zero environmental magnetic field are important conditions to operate the alkali-metal atoms in the SERF regime. On one hand, the cell is installed in a boron-nitride ceramic oven and heated to 453 K by a homemade 199-kHz ac electrical heater. A platinum resistor sensor is used to sample the temperature of the cell stem, and a proportional-integral-differential temperature control system is used to control the cell temperature. On the other hand, the cell and oven are placed in two layers of high-permeability μ-metal cylindrical magnetic shields and an inner MnZn ferrite barrel for shielding the environmental magnetic field, and the residual magnetic fields around the cell are further compensated by the three-axis magnetic coil system.

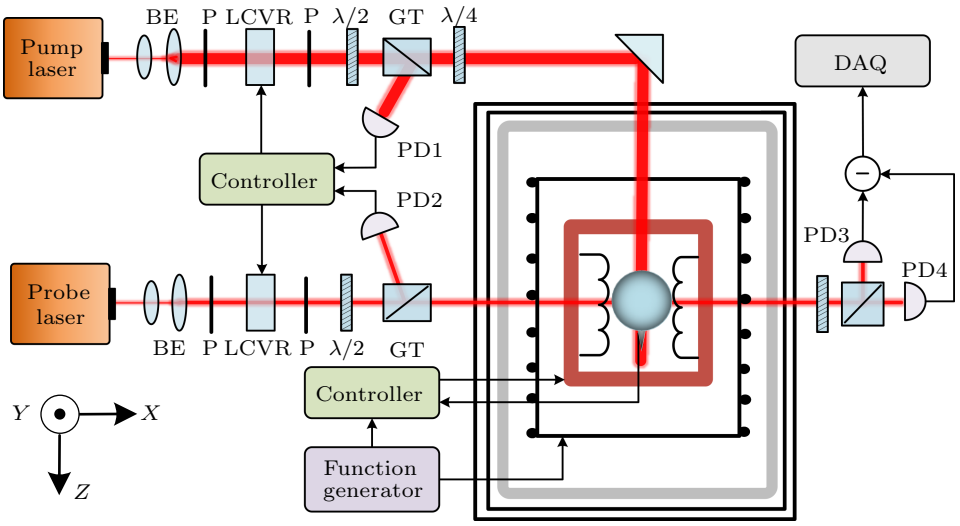



**Fig. 2.** Schematic diagram of the SERF comagnetometer. BE: beam expander; P: linear polarizer; LCVR: liquid-crystal variable retarder; GT: Glan–Taylor polarizer; DAQ: data acquisition system.

The orthogonal pump-probe configuration is adopted in the comagnetometer. The pump laser is emitted from a distributed Bragg reflector (DBR) diode laser with the frequency of D1 line of K atoms. The pump laser is converted to a circularly polarized light and propagate through the cell along $z$-axis to polarize the alkali metal and noble gas atoms. The probe laser is generated by a distributed feedback (DFB) diode laser and converted to a linearly polarized light. The frequency of the probe laser is set to detune with the D1 line of Rb atoms. The probe laser pass through the cell along $x$-axis to detect the precession of the atoms. The power fluctuations of the pump and probe lasers are suppressed by a homemade laser intensity controller. The output signal of the comagnetometer is obtained by the balanced photodetector consisting of the polarizing beamsplitter and photodetectors (PD3 and PD4, Hamamatsu, S1227-66BR), and recorded by a data acquisition (DAQ) system.

## 4. Results and discussion

With several hours of the continuous pumping and heating, the spin coupled ensemble in the cell of the comagnetometer reaches a stable equilibrium state. The temperature coefficient of the SERF comagnetometer is measured, which is obtained by measuring the steady-state response of the comagnetometer with the fluctuation of the cell temperature. The experiment is implemented when the cell temperature is set to 453 K, and the steady-state responses are measured with the temperature range of 452.7 K to 453.3 K, which are shown in Fig. 3(a). The experimental data are fitted by a linear model, and the slope is the temperature coefficient. In order to verify the method for suppression of the vapor cell temperature error, the temperature coefficients with different detuned frequencies of probe laser are measured and summarized in Fig. 3(b).

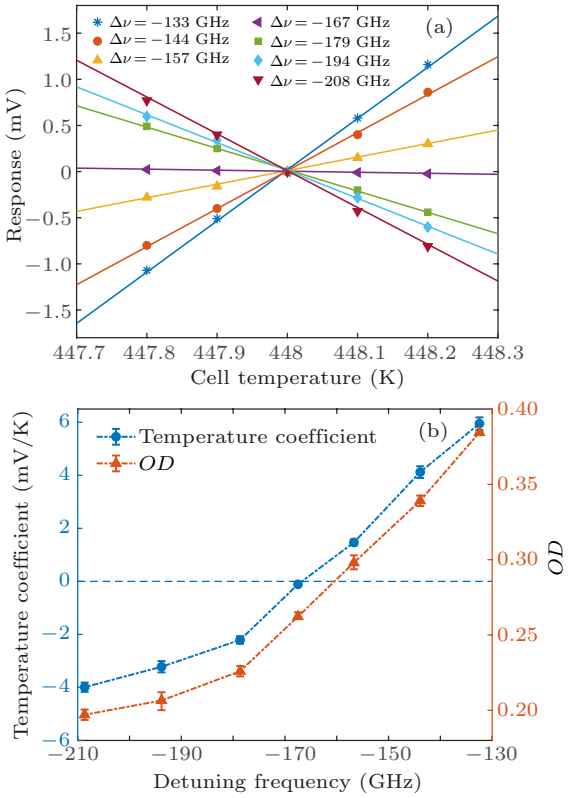



**Fig. 3.** The measurement of the temperature coefficient of the SERF comagnetometer. (a) The steady state responses of the SERF comagnetometer with the fluctuation of the cell temperature, which are fitted by a linear model to obtain the temperature coefficients. (b) The variations of temperature coefficients and *OD* with detuning frequencies, which is coincident with the simulation in Fig. 1.

The *OD* with different detuned frequencies is also measured by detecting the light intensity before and after the cell. The experimental setup for measuring *OD* is modified based on the setup of SERF comagnetometer, where the pump laser of the comagnetometer is turned off. A polarizing beamsplitter (PBS) is added in front of the cell, and a photodetector is used to detect the bypass light intensity of the PBS, which can reflect the light intensity before the cell. The balanced photodetector after the cell in Fig. 2 is taken out, and a photode-

tector is used to detect the light intensity after the cell. The signals of the photodetectors are amplified by the benchtop photodiode amplifier (Thorlabs PDA200C), which is ideally suited for ultra-low-noise amplification of very small photodiode currents. Therefore, the precise measurement of *OD* can be realized in the experimental setup. The corresponding *OD* are also obtained by measuring the probe laser powers before and after the cell, and plotted in Fig. 3(b). The results show that the temperature coefficients change from $-3.99$ mV/K to 5.95 mV/K with the detuning frequency changes from $-208$ GHz to $-132$ GHz. When the detuning frequency is $-167$ GHz, the temperature coefficient is $-0.11$ mV/K, which is approximately zero. And the corresponding *OD* is 0.26, which is coincident with the simulation in Fig. 1 and verify the validity of the method.

For systematically studying the variation of the temperature coefficient with different conditions, the temperature coefficients with different pump laser power densities and temperatures are simulated based on Eq. (6), which are shown in Figs. 4(a) and 4(b) respectively. For convenience, the detuning frequency of the zero point of the temperature coefficient is denoted as $f_0$. The results indicate that $f_0$ increases with the decrease of the pump laser power density and the increase of the cell temperature, which is caused by the relation of the relaxation rate $R_{\rm rel}^{\rm iT}$ and $R_{\rm sd}^{\rm ee}$. In the SERF comagnetometer, the pumping rate $R_{\rm p}$ is the main component of $R_{\rm rel}^{\rm iT}$, which is proportional to the pump laser power density. With the decrease of the pumping optical power density, the difference between $R_{\rm rel}^{\rm iT}$ and $R_{\rm sd}^{\rm ee}$ decreases, which cause to the decrease of *OD* according to Eq. (7). Since *OD* is inverse proportional to the detuning frequency, the $f_0$ increases with the decrease of *OD*. When the relaxation rate $R_{\rm rel}^{\rm iT}$ is smaller than the $R_{\rm sd}^{\rm ee}$, there is no zero point of temperature coefficient, which corresponds to the simulation with the pump laser power densities of 26 mW/cm$^2$ shown in Fig. 4(a). However, the pumping rate $R_{\rm p}$ is typically larger than $R_{\rm rel}^{\rm iT}$ in the comagnetometer for promoting the polarization of the electron and nuclear spins, and suppressing the low-frequency magnetic noise.[26] Consequently, the method for suppressing the temperature fluctuation error proposed in this work is effective in the normal working conditions of the comagnetometer. Similarly, since the relaxation rate $R_{\rm sd}^{\rm ee}$ increases with the temperature, the difference between $R_{\rm rel}^{\rm iT}$ and $R_{\rm sd}^{\rm ee}$ decreases with the temperature, which cause the simulation result in Fig. 4(b). Therefore, $f_0$ can be adjusted by manipulating the pump laser power density and temperature in the comagnetometer.

In order to evaluate the suppression effect of the temperature fluctuation, the long-term stability of the SERF comagnetometer is studied. The output signal of the SERF comagnetometer is recorded for two hours with the sample rate of 200 Hz when the comagnetometer is kept static. The Allan deviation analysis of the output signal with different temperature coefficients is shown in Fig. 5(a). The minimum of the Allan deviation can reflect the bias instability of the SERF comagnetometer. The result indicates that the bias instability is improved as the temperature coefficient decreases, and a bias instability of 0.015 °/h is acquired when the temperature coefficient is approximately zero, which is promoted by 34% compared with the temperature coefficient of 5.95 mV/K. Therefore, the long-term stability of the comagnetometer is improved by 34% after adjusting the comagnetometer to a working point that insensitive to the cell temperature fluctuation.

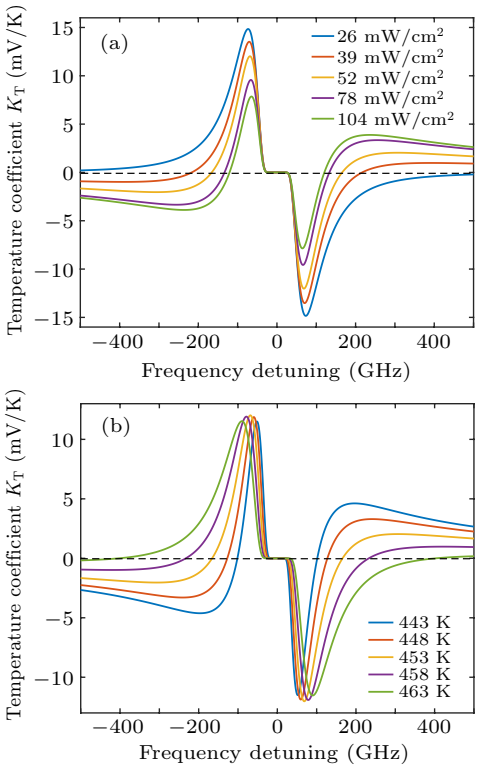



**Fig. 4.** The simulations of the temperature coefficient of the SERF comagnetometer with different pump laser power densities (a) and temperatures (b).

In addition, the sensitivity of the SERF comagnetometer operated at different temperature coefficients are compared and shown in Fig. 5(b), which is obtained by calculating the power spectral density of the 200-s output signal of the SERF comagnetometer and averaging for each 0.05-Hz bin. Similar with the variation of the bias instability with the temperature coefficient, the sensitivity is also improved with the decrease of the temperature coefficient. When the temperature coefficient is approximately zero, the sensitivity of the SERF comagnetometer is $4.3\times10^{-6}$ (°/s)/Hz$^{1/2}$.

The output signal strength of the comagnetometer in the zero point of the temperature coefficient is not the maximum output signal, but this does not mean the decrease of the signal-to-noise ratio. This is because that the noise induced by the fluctuations of cell temperature affects the polarization of electron spins and couples into the output signal, resulting in an

increase in noise as the output signal strength increases. The signal-to-noise ratio of the comagnetometer can be improved by suppressing the cell temperature fluctuation error. Therefore, both the long-term stability and sensitivity of the SERF comagnetometer are improved by suppressing the temperature fluctuation error using this method.

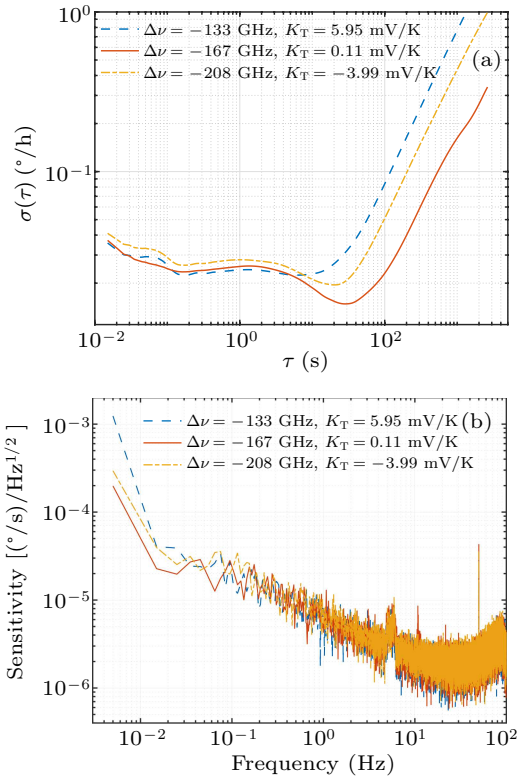



**Fig. 5.** The Allan deviation curves (a) and sensitivity (b) of the SERF comagnetometer operated at different temperature coefficients. The results show that both the long-term stability and sensitivity are improved with the decrease of the temperature coefficient.

## 5. Conclusion

In conclusion, we have proposed a novel method for suppressing the vapor cell temperature error of the SERF comagnetometer by manipulating the probe laser frequency. A temperature coefficient model of the SERF comagnetometer has been established based on the steady-state response to analyze the impact of the temperature fluctuation on the comagnetometer. The results indicate when the *OD* is equal to the ratio of the difference of the relaxation rate of the electron spins independent on temperature and the spin-destruction relaxation rate to the total relaxation of the electron spins, the output signal of the comagnetometer is insensitive to the cell temperature fluctuation. In order to verify this method, the temperature coefficients and *OD* of a K–Rb–$^{21}$Ne comagnetometer with different probe laser frequencies are measured, and the experimental results are consistent with the theory. Based on this method, both the long-term stability and sensitivity of the SERF comagnetometer are improved. The theory and method presented here are beneficial for improving the performance of SERF comagnetometer, and are of great significance to practical applications of the SERF comagnetometer.

## Acknowledgements

Project supported by the National Natural Science Foundation of China (Grant Nos. 62103024 and 61925301), and in part by the Aeronautical Science Foundation (Grant No. 2023Z073051012).

## References

[1] Schreiber K U and Wells J P R 2013 *Rev. Sci. Instrum.* **84** 041101
[2] Belfi J, Beverini N, Bosi F, Carelli G, Cuccato D, De Luca G, Di Virgilio A, Gebauer A, Maccioni E, Ortolan A, Porzio A, Saccorotti G, Simonelli A and Terreni G 2017 *Rev. Sci. Instrum.* **88** 034502
[3] Flambaum V V and Romalis M V 2017 *Phys. Rev. Lett.* **118** 142501
[4] Lee J, Almasi A and Romalis M V 2018 *Phys. Rev. Lett.* **120** 161801
[5] Jiang L W, Liu J L, Liang Y X, Tian M N and Quan W 2022 *Appl. Phys. Lett.* **120** 074101
[6] Xing L, Zhai Y, Fu Y, Song T, Liu F, Cai Q and Quan W 2020 *Meas. Sci. Technol.* **32** 025112
[7] Pei H Y, Fan W F, Du P C, Zhang K, Yuan L L and Quan W 2023 *IEEE Trans. Instrum. Meas.* **72** 1
[8] Kornack T W, Ghosh R K and Romalis M V 2005 *Phys. Rev. Lett.* **95** 230801
[9] Smicikla M, Brown J M, Cheuk L W, Smullin S J and Romalis M V 2011 *Phys. Rev. Lett.* **107** 171604
[10] Jiang L W, Quan W, Liu F, Fan W F, Xing L, Duan L H, Liu W M and Fang J C 2019 *Phys. Rev. Appl.* **12** 024017
[11] Huang J, Wang Z, Fan W F, Xing L, Zhang W J, Duan L H and Quan W 2020 *Opt. Express* **28** 35748
[12] Xu Z T, Wei K, Liu C, Heng X, Huang X F, Gong D, Wang F, Zhai Y Y and Quan W 2024 *IEEE Trans. Instrum. Meas.* **73** 1
[13] Chen Y, Quan W, Zou S, Lu Y, Duan L H, Li Y, Zhang H, Ding M and Fang J C 2016 *Sci. Rep.* **6** 36547
[14] Fang W F, Quan W, Liu F, Duan L H and Liu G 2019 *Chin. Phys. B* **28** 110701
[15] Happer W and Tang H 1973 *Phys. Rev. Lett.* **31** 273
[16] Allred J C, Lyman R N, Kornack T W and Romalis M V 2002 *Phys. Rev. Lett.* **89** 130801
[17] Alcock C B, Itkin V P and Horrigan M K 1984 *Canadian Metallurgical Quarterly* **23** 309
[18] Ito S, Ito Y and Kbayashi T 2019 *Opt. Express* **27** 8037
[19] Fang J C, Wang T, Zhang H, Li Y and Zou S 2014 *Rev. Sci. Instrum.* **85** 123104
[20] Liu F, Duan L H, Fan W F, Pang H Y, Liu S X and Quan W 2022 *IEEE Sens. J.* **22** 1990
[21] Wu J, Liu Feng, Fan W F, Du P and Quan W 2022 *Meas. Sci. Technol.* **34** 15113
[22] Liu F, Wu J and Quan W 2022 *Rev. Sci. Instrum.* **93** 015102
[23] Ruan J S, Duan L H, Fu Y, Fan W F and Quan W 2023 *Opt. Express* **31** 8342
[24] Lu J X, Qian Z Fang J C and Quan W 2015 *Rev. Sci. Instrum.* **86** 083103
[25] Liu J L, Duan L H, Jiang L W, Liang Y X, Tian M N and Quan W 2023 *IEEE Trans. Instrum. Meas.* **72** 1
[26] Jiang L W, Quan W, Liang Y X, Liu J L, Duan L H and Fang J C 2019 *Opt. Express* **27** 27420
[27] Liu J L, Jiang L W, Liang Y X, Liu F and Quan W 2020 *IEEE Trans. Instrum. Meas.* **69** 7805
[28] Jiang L W, Quan W, Li R J, Duan L H, Fan W F, Wang Z, Liu F, Xing L and Fang J C 2017 *Phys. Rev. A* **95** 062103
[29] Chen Y, Quan W, Duan L H, Lu Y, Jiang L W and Fang J C 2016 *Phys. Rev. A* **94** 052705
[30] Liu J L, Jiang L W, Liang Y X, Li G H, Cai Z, Wu Z H and Quan W 2022 *Phys. Rev. Appl.* **17** 014030
[31] Budker D, Gawlik W, Kimball D F, Rochester S M, Yashchuk V V and Weis A 2002 *Rev. Mod. Phys* **74** 1153